RSC Advances

PAPER

View Article Online
View Journal | View Issue

Cite this: *RSC Adv.*, 2015, **5**, 49429

Green and low-cost synthesis of PANI–TiO_2 nanocomposite mesoporous films for photoelectrochemical water splitting†

D. Hidalgo,[ab] S. Bocchini,[a] M. Fontana,[ab] G. Saracco[b] and S. Hernández*[ab]

Received 14th April 2015
Accepted 28th May 2015

DOI: 10.1039/c5ra06734k

www.rsc.org/advances

Among conductive polymers, polyaniline (PANI) has been widely used to improve electronic conductivity, solar energy transfer and photocatalytic activity of TiO_2, due to its ease preparation and excellent environmental stability. In this study, a green and low-cost synthesis procedure was developed for the preparation of PANI–TiO_2 nanocomposite films. A non-toxic and low-cost polymerization route, starting from aniline dimer and polystyrene sulphonate as emulsioning/doping agent in water, was employed to synthesize the conductive form of PANI (emeraldine salt, ES). Anatase TiO_2 nanocrystalline mesoporous films were prepared by a novel and green sol–gel spin coating method, which employs titanium tetraisopropoxide, acetic acid and a nonionic surfactant (Tween 20) in excess of water, avoiding the use of flammable solvents. Uniform PANI–TiO_2 composite films, containing PANI in either ES or pernigraniline base (PB) forms, *i.e.* PANI/TiO_2 and PANIox/TiO_2, respectively, were then prepared by a simple impregnation method. The films were characterized by means of XRD, ATR, FESEM and TEM techniques and their photocatalytic activity was assessed using them as photoelectrochemical water splitting photoanodes. Both PANI/TiO_2 and PANIox/TiO_2 showed an enhanced water oxidation efficiency under AM 1.5G simulated sunlight irradiation, reaching about 2 and 1.6 fold higher photocurrent densities, respectively, than a pure TiO_2 nanoparticles film. They also demonstrated good stability after several hours of operation. UV-Vis spectrophotometry and IPCE analysis reveal the main role of PANI, in the system PANI/TiO_2 for the PEC water oxidation, is as sensitizer of TiO_2 in the UV light by significantly increasing charges separation, electrons transport and collected photoelectrons, indirectly contributing to the generation of O_2. Indeed, PANI-ES photogenerated e^- are transferred to the TiO_2 conduction band while its h^+ can react with OH^- to produce OH radicals that generate H_2O_2, which can subsequently be photooxidized on the TiO_2 NPs surface generating more O_2 than such produced by the direct water oxidation on the TiO_2 holes.

Introduction

Photochemical and photoelectrochemical (PEC) water splitting have been widely investigated in the last decades as a means of converting solar to chemical energy in the form of fuels, providing a viable energy resource with minimal environmental impact after combustion.[1,2] Hydrogen is a key solar fuel since it can be used directly in Proton Exchange Membrane (PEM) fuel cells or combustion engines, or combined catalytically with CO_2 to make carbon containing fuels.[2,3]

The first example for water splitting into hydrogen and oxygen was reported by Fujishima and Honda in 1972,[3] using TiO_2 as photocatalyst under UV light. Subsequently, different semiconductors (*e.g.* ZnO, Fe_2O_3, $BiVO_4$, WO_3) have been reported for the sun-driven water photoelectrolysis.[4] However, the interest in the application of TiO_2 as water splitting photocatalyst and for other uses (*e.g.* photodegradation of contaminants, photovoltaics, electrical energy storage, paint pigments, *etc.*) is still high, due to its non-toxicity, abundance, low-cost, good stability, excellent photocatalytic performance, easy availability and possibility to be structured at the nano- and micro-scales.[5] Indeed, several recent reviews deal with the general approaches toward the fabrication of 3D-titania morphologies,[4,6–8] with a particular interest in porous titania materials,[9–13] porous spheres,[14,15] shells,[16] nanosheets,[17] nanorods,[18] fibers,[19] and nanotubes,[20–22] are focused on various applications of 3D-titania materials in solar cells,[15,23] photocatalysis and photoelectrochemistry[24–28] or electrochemical energy storage.[13] Nevertheless, the disadvantages of TiO_2 with respect to its application as water oxidation photocatalyst are its limited absorption of solar light (wavelengths below ~380 nm) due to its

[a]*Center for Space Human Robotics, Istituto Italiano di Tecnologia, IIT@POLITO, Torino, Italy. E-mail: simelys.hernandez@polito.it; Tel: +39 011 0904774*

[b]*Applied Science and Technology Department, DISAT, Politecnico di Torino, Torino, Italy*

† Electronic supplementary information (ESI) available: *I–t* measurement and GC results for faradaic efficiency calculation. See DOI: 10.1039/c5ra06734k

large bandgap (3.20 eV), and its reduced photocatalytic activity because of the fast recombination of charge carriers.[29] Thus, the capability to design semiconductor photoelectrodes that function as both a photosensitizer and an energy converter, with suitable band edge energies, appropriate spectral response, and good photostability is of fundamental importance.[2]

Efforts to overcome such issues have been made by modifying TiO_2 with methods such as metal and non-metal doping,[25] noble metal deposition,[30] forming composites with both narrow band gap inorganic semiconductors or through dye sensitization.[6,28] Regarding the last approach, in order to warrant a good electron/hole transfer, the bottom of the conduction band (CB) and the top of the valence band (VB) of the semiconductor (or the lowest unoccupied molecular orbital (LUMO) and the highest occupied molecular orbital (HOMO) of the dye) must have higher energy than the ones of TiO_2. There are few inorganic materials satisfying such requirements (*e.g.* CdS,[31] Fe_2O_3 [32]), which in some cases have stability issues, and the application of dye-sensitized TiO_2 is restricted due to the employment of noble-metal-containing dyes (*e.g.* Ru-, Rh- or Pd-containing dyes) or because of dissolution and degradation of dyes during photocatalytic processes.[33–35]

In recent years, polymers with extended π-conjugated electron systems have attracted considerable attention because of their absorption coefficients in the visible region and high conductivity, allowing high mobility of charge carriers. Among conductive polymers, polyaniline (PANI) has been widely used to improve electronic conductivity as well as solar energy transfer and photocatalytic activity of TiO_2, due to its easiness of preparation, comparatively low cost and excellent environmental stability.[36]

From a chemical point of view, as shown in Fig. 1a, PANI can be considered as being derived from two different repeating units, which are alternatively reduced (benzenoid diamine unit) and oxidized (quinoid diimine unit).[37–40] Of the different oxidation states of PANI, only emeraldine (Fig. 1c), the half oxidized form,[34] was proved to be electrical conductive. The mechanism of doping is linked to the protonation of the emeraldine form that is called basic form or emeraldine base (EB). The degree of protonation of the polymeric base depending on its oxidation state and on the pH of the aqueous acid, because complete protonation of the imine nitrogen atoms in EB results in the formation of a delocalized polysemiquinone radical cation.[38,39,41]

In the available literature different ways to produce PANI have been demonstrated, however, aniline is classically chosen as the starting monomer. In previous works,[42,43] a method to produce polyaniline in the EB form starting from the aniline dimer (DANI), which on the contrary to aniline is non-toxic and low-cost, was developed. Such method produces PANI soluble in organic solvents, which thus can be used to functionalize other materials (*e.g.* titanium oxide) by drop casting and impregnation, among other techniques.

A high number of works exploit the role of PANI–TiO_2 composites for photocatalytic degradation or organic matrix[30,33,44–49] by generation of $OH^{\bullet}$ radicals or for photovoltaic solar cells.[50] On the other hand, there are some examples of PANI

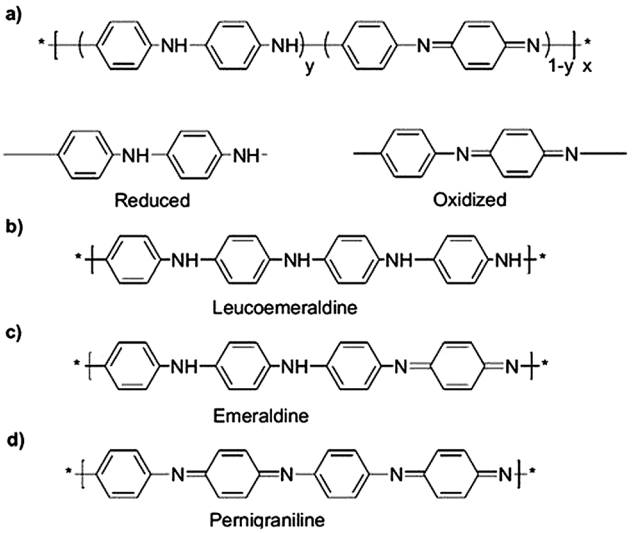

Fig. 1 Generalized composition of polyanilines indicating the reduced and oxidized repeating units (a), the completely reduced polymer (b), the half-oxidized polymer (c) and the fully oxidized polymer (d). Reproduced and adapted from ref. 37.

combined with other semiconductors for H_2 generation, such as the case of PANI–CdS composite nanoparticles synthesized by He *et al.*[51] for direct H_2 evolution in the presence of SO_3^{2-}/S^{2-} sacrificial reactant. Nevertheless, there are few examples of PANI-semiconductor supported composites tested for the PEC water splitting reaction. Only recently, Jing *et al.*[29] reported on a ternary polyaniline–graphene–TiO_2 hybrids for water oxidation in Na_2SO_4 (pH = 7) electrolyte under visible light illumination generating up to 10 μA cm^{-2} at 0.8 V *vs.* SCE (~1.4 V *vs.* RHE).

In this study, we report for the first time the synthesis of PANI–TiO_2 nanocomposite mesoporous films prepared through a simple, safe, low-cost and environmentally friendly procedure. A non-toxic and low-cost oxidative polymerization route, which starts from aniline dimer (instead of the usually employed aniline) was applied to synthesize PANI in its emeraldine salt (ES) conductive form.[42] Polystyrene sulphonate was used as emulsioning/doping agent of PANI in aqueous solution, so that PANI could remain stable also under high pH values. On the other hand, TiO_2 films were prepared using environmentally friendly precursors (*i.e.* titanium tetraisopropoxide, acetic acid, the nonionic surfactant Tween 20 and water as solvent).[52] Starting from such materials, the 3D mesoporous TiO_2 nanoparticles films were impregnated *in situ* with the ES PANI solution, obtaining a uniform surface coverage of the mesoporous substrate after only ten minutes (*i.e.* PANI/TiO_2 sample). In addition, an oxidized PANI–TiO_2 sample (*i.e.* PANIox/TiO_2) was prepared by immersion into an aqueous solution of sodium persulfate, in order to investigate the role of the thus formed pernigraniline base form of PANI in the photocatalytic behavior of the nanocomposite samples.

The PANI–TiO_2 nanocomposites were fully characterized in their physico-chemical characteristics, and their photocatalytic activity was proved by evaluating their PEC behavior for the water splitting reaction under simulated solar light (AM 1.5G).

Results and discussion

Physico-chemical characterization of TiO_2 and PANI–TiO_2 films

A typical X-ray diffraction spectrum of a TiO_2 film is illustrated in Fig. 2. The TiO_2 film was prepared with 1 spin coating layer using a molar ratio between Tween 20/TTIP of 0.50/1 in the sol. The XRD patterns present peaks at 25.4° (101) and 47.7° (200), corresponding to the anatase phase, which is the most active phase of TiO_2 for several photocatalytic applications.[9,44] The X-ray diffraction patterns of both PANI/TiO_2 and PANIox/TiO_2 nanocomposite films (not shown) are similar to the one of the TiO_2 NPs film. Thus, impregnation with PANI had no influence on the crystallinity of the TiO_2 NPs.

FESEM analysis was used to investigate the morphology and the adhesion of the TiO_2 and TiO_2–PANI films to the substrate. As can be seen from Fig. 3a and b, the pristine TiO_2 films are homogeneous and crack-free along the whole surface, and show good adhesion to the substrate. All the prepared TiO_2 films have a thickness of about 530 nm (see Fig. 3b) and are constituted by nanoparticles with average size in the range (10–20) nm, which are organized in a mesoporous structure. The results from this analysis are consistent with a previously published work.[9]

Further insight into the morphology and crystalline structure of the nanoparticles was obtained through TEM characterization. Fig. 3c presents a selected area electron diffraction pattern (SAED), which confirms that the samples are constituted by polycrystalline anatase TiO_2, as evidenced by the presence of diffraction rings. By the analysis of high resolution TEM images (Fig. 3d), it can be seen that the nanoparticles are single crystals, with average size consistent with the previous FESEM morphological measurements. Concerning the characterization of the impregnated samples, PANI/TiO_2 was initially analyzed by FESEM (Fig. 3e). From the morphological point of view, there are no significant changes with respect to the TiO_2 NPs film, suggesting that the PANI layer on the TiO_2 is very thin. This assumption is in accordance with high-resolution TEM images: Fig. 3f shows the presence of a thin layer (<5 nm) of amorphous material surrounding the nanoparticles, which can be ascribed to surface coating of the TiO_2 sample with PANI. Nevertheless, no information about the 3-dimensional location of PANI with respect to the mesoporous TiO_2 film can be inferred from TEM analysis, as a consequence of the samples preparation. It seems reasonable to assume that the PANI-covered TiO_2 NPs are mostly located near the surface of the film, because of the limited interpenetration of the high molecular weight polymer in the mesoscopic structure. Further proof of the presence of PANI in the samples was obtained by FT-IR spectroscopy.

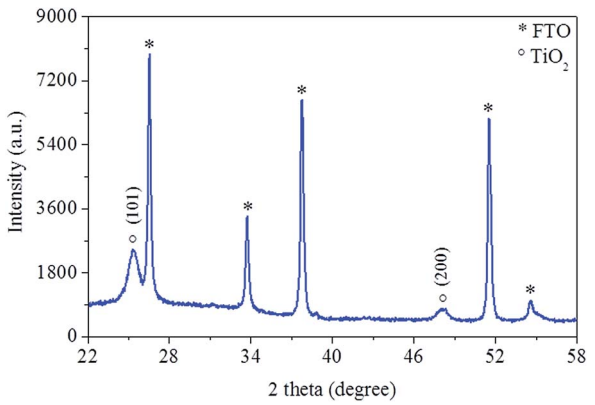

Fig. 2 XRD spectrum for immobilized TiO_2 film calcined at 500 °C.

The experimental FT-IR spectra in ATR mode of both the TiO_2 film and the PANI–TiO_2 films, before and after preliminary oxidation, are reported in Fig. 4. Due to the low signal obtained on ATR with the TiO_2 films impregnated in 2 wt% of PANI solution, the FT-IR spectra reported in Fig. 4 correspond to TiO_2 films impregnated with a 10 wt% PANI solution, which were used only for characterization purposes. These spectra confirm the presence of PANI in the TiO_2 films and allow the analysis of the PANI oxidation state.

The TiO_2 is well identified by two main absorbance peaks in the (OH) stretching region (3100–4000 cm^{-1}). The broad band at 3400 cm^{-1} is associated with weakly bonded hydroxyl groups, while the absorbance peak at 3747 cm^{-1} is characteristic of non-hydrogen bonded hydroxyl groups.[53] The other band with a maximum at 818 cm^{-1} is associated to vibration of bulk TiO_2 skeletal frequency region.[37]

Regarding the samples PANI/TiO_2 and PANIox/TiO_2, ATR spectra present the absorbances already described for the TiO_2 film. In addition, the PANI characteristic absorbance peaks are well distinguishable but practically super-imposable in both samples, thus meaning that the oxidation process in the sample PANIox/TiO_2 does not degrade the PANI skeletal structure. The 1308 cm^{-1} band is a fingerprint associated with the C–N stretching typical of PANI.[38] The band at 1567 cm^{-1} attributed to C=N stretching of quinoid diimine unit (the oxidised form of PANI). C–C aromatic ring stretching of the benzenoid diamine unit (the reduced form of PANI) appears at 1494 cm^{-1}.[54] Based on previous reports, the intensities presented by these last two absorption bands should identify the oxidation state of PANI.[52] Indeed, the ratio between such intensities is indicative of the extent of oxidation state of the polymer, which evidence the content of the quinoid diimine with respect to the benzene ring structure. The ratio is calculated as follows: R (intensity ratio) = $(I_{quinoid})/(I_{benzenoid})$, where I is the absorption intensity. Obviously, the higher is the ratio the higher is oxidation number. In this case R is equal to 0.6 for the PANI/TiO_2 sample and 0.65 for the PANIox/TiO_2 film, thus indicating a partial transformation from emeraldine to pernigraniline form after the pre-oxidation of the sample. The difference between the intensity of bands is low, since the oxidation is limited to a very thin layer while the ATR includes a thicker layer in which oxidation does not occur. This finding is supported by the fact that the PANI/TiO_2 changed its color from green (typical of emeraldine salt, ES) to violet (distinctive of pernigraniline form of PANI) after oxidation in the sample impregnated with the 2 wt% solution that has a thinner layer of PANI on the surface. In the latter case, it can be supposed

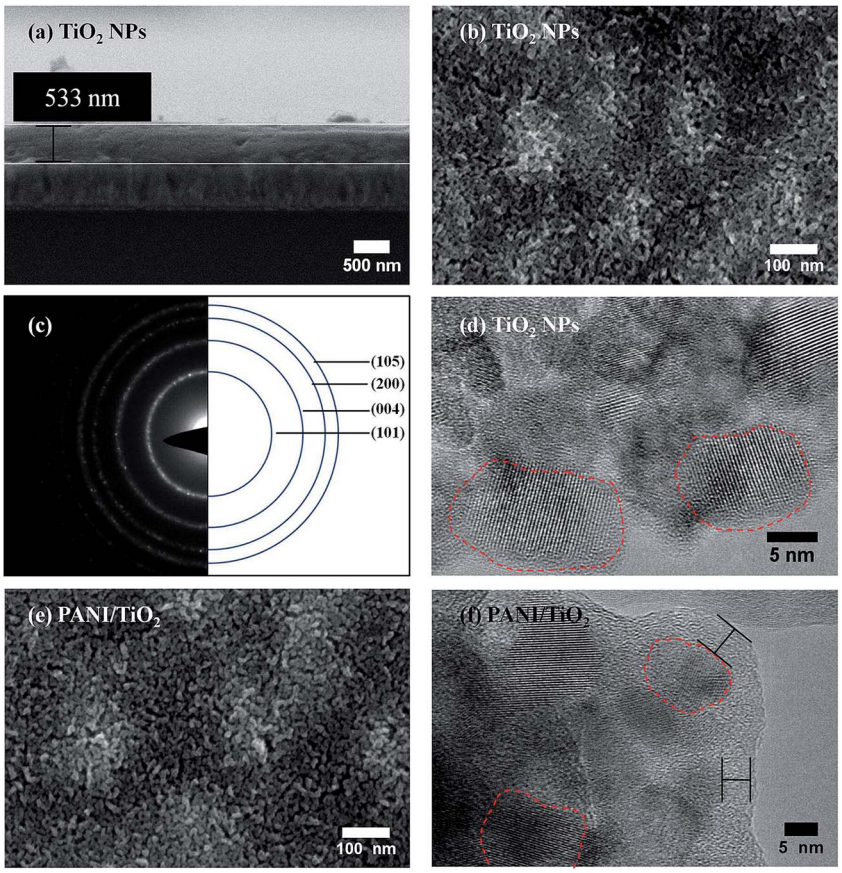

Fig. 3 FESEM images of TiO_2 film in cross-section (a) and top view (b). Fragments of the film on the surface of the sample in (a) are due to sample preparation for cross-section imaging. SAED pattern of the TiO_2 sample corresponding to polycrystalline anatase TiO_2 (c). HRTEM image of the TiO_2 sample (d). Top-view FESEM image (e) and HRTEM image (f) of the PANI/TiO_2 sample.

that pernigraniline is in the base form, mainly because it is stable only in really acidic conditions (*e.g.* at pH near to 0).[55] Although this analysis is only qualitative when using ATR infrared spectra, since this method is usually applied by using the absorbance obtained from FT-IR analysis in transmittance mode, it provides a good approximation for comparative purposes.

Photoelectrochemical characterization of TiO_2 and PANI–TiO_2 films

The PEC behavior of the TiO_2 NPs, PANI/TiO_2 and PANIox/TiO_2 composite films were evaluated using the prepared photoanodes for the water photoelectrolysis reaction in 0.1 M NaOH solution (pH = 12.7). From LSV scans in dark conditions shown in Fig. 5a, only a slight current (<0.1 μA cm^{-2}) was

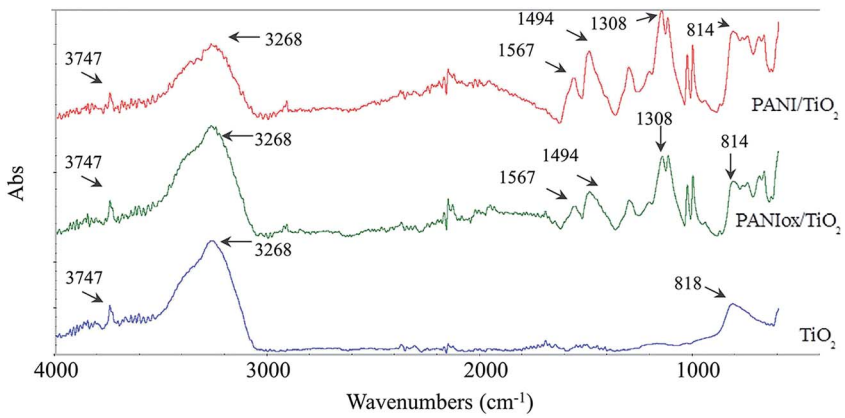

Fig. 4 ATR infrared spectra of TiO_2 and PANI–TiO_2 films.

measured for all the samples, due to the high overpotential effect of both TiO_2 semiconductor and PANI–TiO_2 composites in the absence of illumination. In contrast, under simulated sunlight irradiation (AM 1.5G, 100 mW cm^{-2}), a sudden increase of the photocurrent is observed for all the samples, at potentials more negative than the theoretical redox potential for water oxidation ($E^o = 1.23$ V *vs.* RHE), which indicates that part of the energy required for the reaction is provided by light. These results are in agreement with the expected behavior for a n-type semiconductor.[56] The photocurrent density (J) of the TiO_2 NPs photoelectrode showed an important rise starting at about 0.56 V *vs.* RHE, reaching a maximum J value of 6.08 μA cm^{-2} at about 1.68 V *vs.* RHE, which is associated with the saturation of the TiO_2 semiconductor.[9,57,58] In contrast, the PANI/TiO_2 and PANIox/TiO_2 photoelectrodes showed a pronounced increase of J starting at about 0.58 and 0.77 V *vs.* RHE, respectively, which continue to rise until reaching maximum values of correspondingly 12.10 and 10.03 μA cm^{-2} at 1.68 V *vs.* RHE. The different feature of both PANI/TiO_2 and PANIox/TiO_2 could be explained by the different photocatalytic and transport properties of such nanocomposite materials with respect to the TiO_2 NPs, as will be discussed below. Such results are of high relevance if compared with the recently reported PANI–graphene–TiO_2 ternary composite electrode, with which a maximum photocurrent of 10 μA cm^{-2} (at about 1.4 V *vs.* RHE) was obtained for the water photoelectrolysis reaction,[29] thanks to the faster electron transfer rate attributed to the introduction of well-conductive graphene and PANI.

In addition, Fig. 5b shows the photocurrent density of the investigated photoanodes as a function of time, after different cycles of darkness and UV-Vis illumination. The anodic photocurrent increase immediately after the light was turned on, due to instantaneous photoinduced electron transition from the VB to the CB of the semiconductor, and then a slight decrease is observed until a steady state value is reached. The steady state photocurrent for the PANI/TiO_2 sample doubled the TiO_2 NPs film performance and it is about 30% higher than the one of the PANIox/TiO_2 film, in accordance with LSV results. As expected, when the light was turned off, the photocurrent decreased quickly down to zero, confirming the effective photocatalytic (and not only catalytic) activity of all the studied materials.

The increase in the photocatalytic activity of PANI/TiO_2 and PANIox/TiO_2 compared to TiO_2 NPs should be essentially attributed to a more efficient separation and transport of charge carriers, as explained in following.

Fig. 6 illustrates the processes of photoexcitation, charge separation and reaction in the PANI–TiO_2 composite film system, under UV-Vis illumination. In such case in which PANI is in the ES form, the HOMO of PANI is the polaron band, while its LUMO is the π* band. Hence, when the PANI–TiO_2 composite film is irradiated with UV-Vis light, PANI absorbs photons, and electrons in the HOMO can be excited to the LUMO. In the same manner, TiO_2 absorb UV photons and electrons in the VB of TiO_2 can be excited to its CB, thereby leaving holes at its surface able to split water (OH^- in basic media) to O_2. Since the LUMO of PANI is at an energy level

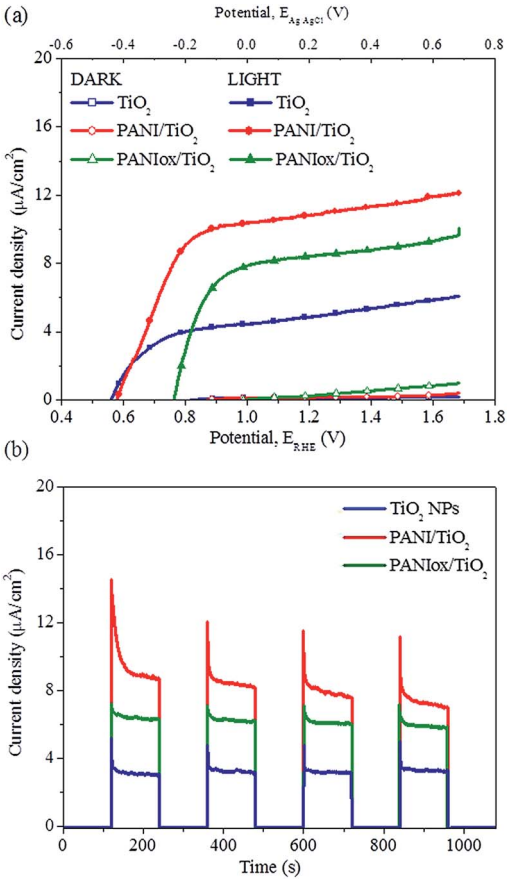

Fig. 5 Photoelectrochemical characterizations for the samples: TiO_2 film (blue line), PANI/TiO_2 film (red line) and PANIox/TiO_2 (green line). (a) LSV collected with a scan rate of 10 mV s^{-1} in the dark and under illumination (AM 1.5G, 100 mW cm^{-2}) and (b) chrono-amperometric (I–t) curves at an applied potential of −0.1 V *vs.* Ag/AgCl under illumination with 120 s light ON/OFF cycles.

higher than such of TiO_2,[59] electrons can be easily injected into the CB of TiO_2, which is advantageous for efficient charge carrier separation due to the increased electrons mobility and transport in the TiO_2 CB.[29] Indeed, electrons in the CB of TiO_2 are then fastly transferred into the FTO conductive substrate, and directed through the external electrical circuit to be used for the H_2 formation reaction at the Pt cathode.

On the other hand, electrons in the TiO_2 VB can also migrate to the HOMO of PANI and recombine with PANI holes, while the holes generated in the TiO_2 VB move to its surface.[33] Otherwise, photogenerated holes formed in PANI remains on its surfaces independently and can react with OH^- groups in water to form OH radicals. This reactivity of PANI has been already suggested in previous works in which TiO_2–PANI composites have been used for the photocatalytic degradation of organic compounds.[44,45,60] OH radicals are highly reactive and, in absence of other species, can couple with another OH radical to form H_2O_2.[61] Hydrogen peroxide is known to decompose spontaneously to O_2 and water, but H_2O_2 can also be photooxidized by holes in TiO_2.[62–64] In conclusion, photogenerated holes formed in both TiO_2 and PANI, following different

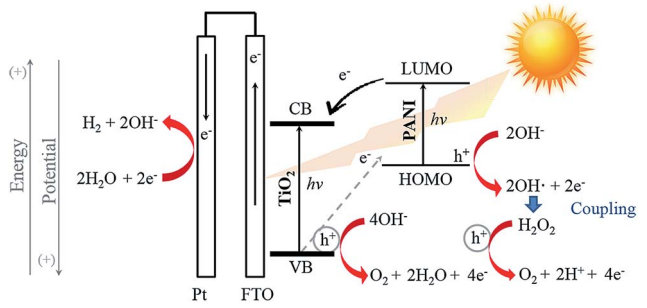

Fig. 6 Mechanism of UV-Vis light absorption and charges transfer in PANI–TiO_2 composite films for the photoelectrochemical water splitting reaction in basic media.

pathways, can react with water (or OH^- ions) to form O_2 which results in higher number of collected photoelectrons,[65–67] then used for the H_2 production in the cathodic electrode. Moreover, PANI itself is unable to split water toward O_2 due to the unfavorable position of the HOMO with respect to the O_2/H_2O redox potential,[68] which is supported by a control test in which no photocurrent was observed using a PANI/FTO electrode under the same PEC conditions. Hence, it is supposed that the TiO_2 activation by UV light is essential in the previously explained mechanism, as it was also confirmed by IPCE measurements shown below.

The sample PANIox/TiO_2 was moreover prepared and tested with the aim to discern if the PANI in the NaOH solution is oxidized, and how this influence the photocatalytic activity of the PANI/TiO_2 film. The results reported in Fig. 5 show that the PANIox/TiO_2 film perform worse than its original counterpart. The difference between PANI/TiO_2 and PANIox/TiO_2 can be easily explained taking into account the presence of some pernigraniline base (PNB) form of PANI in the oxidized material. In the case of PNB the benzenoid orbitals are the LUMO,[69] which have an energy much lower than the π^* band previously considered for the ES, and similar to the TiO_2 CB bottom. Hence, when the PANIox absorbs UV-Vis light, the electrons in the PNB π^* band can undergo more easily to internal relaxation to the PNB benzenoid orbital, thus causing internal recombination.

On the other hand, the open circuit voltage (OCV) of the LSV measurements, *i.e.* the voltage corresponding to $J = 0$, is an approximated measure of the flat band potential (E_{FB}),[70] which is close to the CB in n-type semiconductors such as the titania[71] and to the VB in p-type semiconductors such as the PANI.[68] In addition, E_{FB} determines the band edge positions at the semiconductor–electrolyte interface, thus fixing the energies of conduction band electrons and valence band holes reacting with the electrolyte solution.[71] In the TiO_2–PANI solid interphase a p–n junction is formed.[68] Since the TiO_2 CB is close to the HOMO (VB) of PANI in the ES form,[30] the PANI/TiO_2 flat band potential remains close to that of the TiO_2 film (see Fig. 5a). Instead, the shift towards higher OCV values for the PANIox/TiO_2 is due to the lower HOMO band of the PNB than that of the ES,[69] which induces a more positive flat band potential for this composite film than for the PANI/TiO_2 (represented in Fig. 6). This fact further explains the lower photocatalytic activity of the PANIox/TiO_2 film.

In order to identify the portion of the solar spectra that is actually working in the TiO_2 and PANI–TiO_2 films, both UV-Vis and IPCE spectra were recorded and are reported in Fig. 7. From the UV-Vis spectra in transmittance mode (see Fig. 7a), no significant differences are observed for the TiO_2 NPs, PANI/TiO_2 and PANIox/TiO_2 films between 300 and 330 nm. In this region, high UV light absorption (low transmittance) is observed for all the samples. Between 330 and 420 nm the transmittance increased, indicating a probably related reduction of absorption of the TiO_2 NPs. However, the PANI impregnated samples showed an absorption higher than the pristine TiO_2 NPs in the UV region up to 420 nm, in the following order: PANI/TiO_2 > PANIox/TiO_2 > TiO_2 NPs.

The photoresponse of the different photoanodes evaluated through IPCE spectra at an applied potential of 0.26 V *vs.* Ag/AgCl (1.23 V *vs.* RHE) are reported in Fig. 7b. IPCE curves revealed that either the TiO_2 NPs or the PANI–TiO_2 nanocomposites here prepared have a relevant efficiency only in the UV region up to maximum 390 nm. The maximum IPCE was obtained at 320 nm for all the samples being 6.27%, 8.17% and 10.07% for the TiO_2 NPs, PANIox/TiO_2 and PANI/TiO_2 samples, respectively. These results are in agreement with the highest UV absorption of the PANI impregnated samples, but suggest that

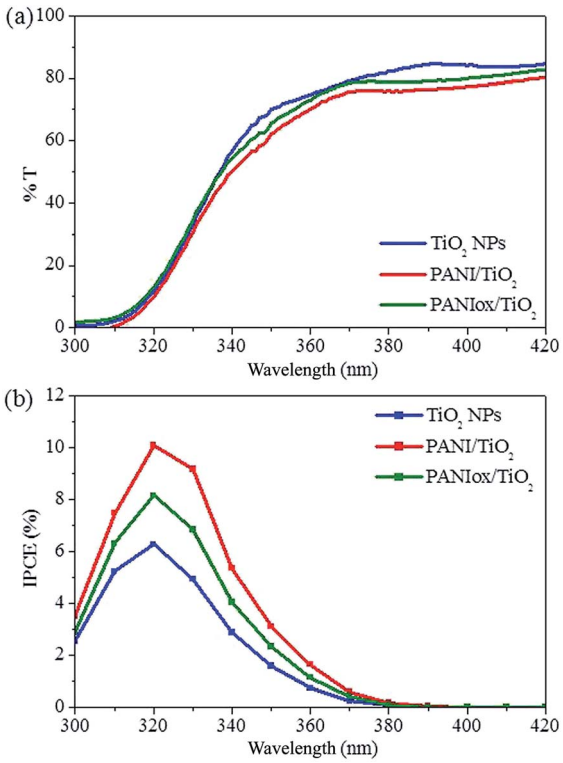

Fig. 7 Optical properties for the samples: TiO_2 film (blue line), PANI/TiO_2 film (red line) and PANIox/TiO_2 (green line). (a) UV-Vis spectra recorded in transmittance mode and (b) IPCE spectra recorded by varying the wavelength of the incident light from 300 nm to 420 nm at an applied potential of 0.26 V *vs.* Ag/AgCl (1.23 V *vs.* RHE).

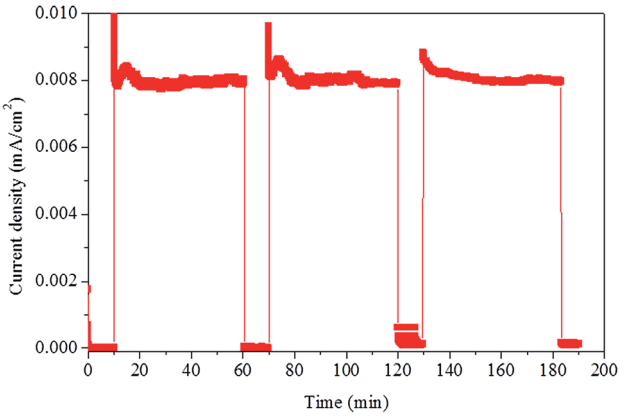

Fig. 8 Photocurrent stability *vs.* time of PANI/TiO_2 film obtained by chrono-amperometric (*I*–*t*) technique at an applied potential of 0.26 V *vs.* Ag/AgCl (1.23 V *vs.* RHE) under illumination with ON/OFF cycles.

for the anodic water splitting reaction the role of PANI in the PANI–TiO_2 composite is more important in the UV than in the visible region of light.

In the literature is reported that PANI plays also a role as sensitizer in the visible region for another redox reactions. For instance, PANI–TiO_2 composite particles, photoexcited with either UV or visible light, have been reported to be effective for the photodegradation of organic compounds (*i.e.* Rhodamine B and Methylene blue), which involves the oxidation of water to OH radicals.[45,60] In the present case, since the water oxidation requires holes with a higher oxidation potential, holes photogenerated in PANI are not able to perform the water oxidation reaction by themselves.[68]

Therefore, the here reported results suggest that the main role of PANI, in the system PANI/TiO_2 for the PEC water oxidation, is as sensitizer of TiO_2 NPs in the UV light by significantly increasing charges separation, electrons transport and collected photoelectrons, and indirectly contributing to the generation of O_2 (in a synergic reaction mechanism that involve photogenerated TiO_2 holes, see Fig. 6), which result in an improved photocatalytic activity.

Finally, after more than 4 hours of operation under photoelectrochemical conditions, the stability of the PANI/TiO_2 nanocomposite photoanode was further assessed by using a chronoamperometric test. Fig. 8 shows the *I*–*t* curve after several hours of operation at −0.1 V *vs.* Ag/AgCl (0.86 V *vs.* RHE). This potential was chosen as a representative value in the region of photocurrent saturation of the sample. A good photocurrent stability was observed under numerous light ON–OFF cycles for a long period of time (about 200 min), thus confirming: a high degree of electrochemical durability, the absence of photodegradation of the ES form of PANI under a highly oxidizing media (thanks to the use of PSS as dopant), and the good adhesion of the PANI/TiO_2 nanocomposite material to the substrate. Moreover, from *I*–*t* and GC analysis (see Experimental and Fig. S1 in the ESI†) it was estimated that the faradaic efficiency of the PANI/TiO_2 film for the H_2 production is almost 100%.

Experimental

Sol–gel synthesis and deposition of TiO_2 nanoparticles

Titanium(IV) isopropoxide (TTIP, 97%), glacial acetic acid (99.7%) and Tween 20, all from Sigma Aldrich, were used as purchased for the preparation of the sol of TiO_2 nanoparticles. The synthesis procedure used to obtain the nano-TiO_2 sol is as follows: TTIP, glacial acetic acid and water were maintained in molar ratios 1 : 10 : 300,[9] whereas a molar ratio (*R*) between Tween 20/TTIP of 0.5/1 was used. Firstly, the TTIP was hydrolyzed into the glacial acetic acid and then, surfactant Tween 20 was added under vigorous stirring. Subsequently, the mixture was added drop wise into the DI-water and the final solution was aged under continuous stirring for 48 h at ambient temperature. Then, the TiO_2 sol was treated in a rotary evaporator at 40 °C for 2 h under vacuum. The final solution was homogeneous and stable for weeks and it was used to the preparation of TiO_2 nanoparticles (NPs) films. TiO_2 films were supported onto Fluorine-doped Tin Oxide glass (FTO, 7 Ω sq^{-1} by Solaronix) substrates in an effective surface area of 4 cm^2. First, the substrate was cleaned in acetone using an ultrasonic bath and then rinsed with ethanol. A "piranha" solution 3 : 1 (sulfuric acid : hydrogen peroxide) was then employed to remove organic residues on the surface. A single layer of the concentrated TiO_2 solution, obtained after the rotary evaporator treatment, was spin-coated with a spinner model Spin 150 by using a two-step program: 1500 rpm for 10 s followed by 3000 rpm for 10 s. Finally, TiO_2 films were annealed in a programmable furnace at 500 °C for 15 min in air, using a heating rate of 1 °C min^{-1}, and were cooled down naturally. Further details of the synthesis and characterization of the TiO_2 films are described elsewhere.[9]

Polyaniline synthesis

N-Phenyl-1,4-phenylendiamine 98%, that is the aniline dimer (DANI), poly(sodium 4-styrenesulfonate) (PSS), ammonium persulfate (APS) 98%, sodium persulfate (SPS) 98%, hydrochloric acid 37 wt%, dimethylsulfoxide (DMSO) 99.9% and dimethylformamide (DMF) were purchased from Aldrich and used as received.

The synthesis of PANI PSS-doped was already presented elsewhere by Bocchini *et al.*[42] PSS was used as emulsioning and doping agent, so that PANI could remain stable also under the high pH conditions used for the PEC tests. In a typical synthesis, 40 mL of a solution of DANI (4 mmol, 0.9212 g) in DMSO was added drop by drop to 360 mL of a solution of PSS (0.915 g) in HCl 0.1 M. After that, a solution of APS (5 mmol, 1.141 g) in 100 mL of HCl 0.1 M was poured slowly. After 3 hours, the precipitate was filtered and washed several times with distilled water. The product was a green powder, which was firstly separated by filtration, then washed with both double distilled water and ethanol, and finally dried at 60 °C until constant weight.

Deposition of polyaniline on TiO_2 films

PANI was deposited in the TiO_2 films by impregnation method. The PANI was dispersed in DMSO at a concentration of 2 wt%

(or 10 wt% for chemical analysis purposes) by alternative mechanical mixing and sonication. Just before use, the PANI solution was ultrasonicated for one hour in order to re-disperse it. The TiO_2 film was dipped into the PANI solution and then removed after 10 min of impregnation. Finally, PANI/TiO_2 composites films were dried at 80 °C under vacuum for 24 h to remove all the residual DMSO. Oxidized PANI/TiO_2 (PANIox/TiO_2) was obtained by immersion of another similarly produced sample in a solution 0.018 M of SPS in water for 1 h.

Materials and characterization

X-ray diffraction (XRD) analysis was performed by using a X-ray diffractometer Cu-Ka X-ray tube ($\lambda = 1.54$ Å) with an accelerating voltage of 40 kV, in order to determine the crystal structure and crystallinity of the TiO_2 particles. Field Emission Scanning Electron Microscopy (FESEM) examinations were performed with a Zeiss Auriga dual beam FIB-SEM microscope. Regarding FESEM sample preparation for cross-section analysis, the films were dipped in liquid nitrogen and subsequently cut. Transmission Electron Microscopy analysis was carried out with a FEI Tecnai F20ST operating at 200 kV. Concerning TEM sample preparation, portions of the samples were detached by mechanical action and subsequently dispersed in ethanol (purity >99.8%, Sigma-Aldrich). After sonication for 5 min, the samples were immediately inserted in the TEM column for the analysis. Attenuated Total Reflectance (ATR) spectra were collected on a Nicolet 5700 FTIR Spectrometer (ThermoFisher) equipped with a ZnSe single crystal. A spectrophotometer model Cary 500 by Varian was used to obtain the UV-Vis transmittance spectra of the samples, which were recorded in the wavelength range of 300–800 nm at room temperature.

Photoelectrochemical tests of TiO_2 and PANI–TiO_2 composites films

The PEC experiments were performed in a glass reactor equipped with a quartz window for frontal illumination.[9] All the tests were carried out in a three electrodes configuration using the TiO_2 NPs, PANI/TiO_2 and PANIox/TiO_2 nanocomposite films as the working electrodes for the water photoelectrolysis reaction, a platinum wire as the counter electrode, and an Ag/AgCl (KCl 3 M) as the reference electrode, in 0.1 M NaOH aqueous electrolyte (pH = 12.7). The electrochemical measurements were performed using a multi-channel VSP potentiostat/galvanostat (by BioLogic), with EC-Lab® software (version 10.1x) for data acquisition. The current–voltage (*I–V*) characteristic curves were recorded by means of Linear Sweep Voltammetry (LSV) at a scan rate of 10 mV s^{-1}, when a constant open circuit voltage was achieved, varying the applied potential from −0.7 V to 0.7 V *vs.* Ag/AgCl, in the dark and under 100 mW cm^{-2} of simulated sunlight (using a 450 W Xe lamp by Newport with an AM 1.5G filter and a water filter model 6123NS). The irradiance was measured by means of a Delta Ohm Photo-radiometer model HD2102.1. Chronoamperometric (*I–t*) tests were carried out to examine the photoresponse of the nanostructures over time at −0.1 V *vs.* Ag/AgCl (0.86 V_{RHE}) under continuous ON–OFF light cycles, with the same illumination condition used for the LSV. The measured potentials *versus* the Ag/AgCl reference electrode were converted to the reversible hydrogen electrode (RHE) scale *via* the Nernst eqn (1):

$$E_{RHE} = E_{Ag/AgCl} + 0.059pH + E^{o}_{Ag/AgCl} \quad (1)$$

where E_{RHE} is the converted potential (V *vs.* RHE), $E_{Ag/AgCl}$ is the experimental potential measured against the Ag/AgCl reference electrode (V *vs.* Ag/AgCl), and $E^{o}_{Ag/AgCl}$ is the standard potential of Ag/AgCl (KCl 3 M) at 25 °C (*i.e.* 0.21 V). Incident photon-to-electron conversion efficiency (IPCE) spectra were recorded using a Newport Xe lamp (150 W) coupled to a monochromator (Cornestone 130 by Newport), by varying the wavelength of the incident light from 300 nm to 550 nm (step size: 10 nm), at an applied potential of 0.26 V *vs.* Ag/AgCl (1.23 V *vs.* RHE). In this case, the electrode illuminated area was 1 cm^2 and the light power density was about 1 mW cm^{-2} (measured at 390 nm). The faradaic efficiency (FE = mol of H_2 theoretically produced/mol of H_2 measured × 100%) was calculated from the data of an amperometry at 0.6 V *vs.* Ag/AgCl for 10 min under light conditions, in order to produce enough gas to be measured within the sensibility of the micro-gas chromatograph (Varian 490 GC, equipped with a Molsieve 5A column of 10 m and a micro-TCD detector) used for the analysis, after outgassing of the cell with an Ar flow rate of 25 NmL min^{-1} (controlled by a Bronkhorst mass flow controller) under continuous stirring.

Conclusions

In order to improve the photocatalytic activity of TiO_2 NPs, PANI–TiO_2 nanocomposite films have been successfully prepared by a simple impregnation method, employing two easy and environmentally friendly synthesis techniques for preparation of both TiO_2 films and PANI conductive polymer. According to FESEM and TEM observations, a thin film of PANI was deposited in the surface of the TiO_2 NP films, which did not significantly alter the morphology and crystallinity of TiO_2 NPs, as was also confirmed by XRD analysis. ATR results confirmed the presence of PANI under the form of emeraldine salt and a mixture of ES and pernigraniline base in the PANI/TiO_2 and PANIox/TiO_2 nanocomposite films, respectively. A remarkable enhancement of the photocatalytic activity was achieved by employing such PANI–TiO_2 nanocomposite films for the PEC water splitting reaction. The PANI/TiO_2 and PANIox/TiO_2 electrodes showed a pronounced increase of the photocurrent under simulated sunlight irradiation (AM 1.5G, 100 mW cm^{-2}), reaching maximum photocurrent densities around 2 and 1.6 fold higher than the pristine TiO_2 NPs. These results are in good agreement with IPCE measurements, which revealed that the PEC activity of both PANI/TiO_2 and PANIox/TiO_2 films was enhanced in 1.6 and 1.3 fold higher with respect to the pristine TiO_2 NPs film at 1.23 V *vs.* RHE. From the results reported in this work, the best performance of the PANI/TiO_2 sample could be associated to an enhanced electrons transport and charges separation, thanks to an increase of e^- in the TiO_2 CB and the generation of H_2O_2 : PANI-ES photogenerated e^- are transferred to the TiO_2 conduction band (due to the proper alignment

between the CB of TiO_2 and the LUMO of PANI) while the h^+ reacts with OH^- to produce OH radicals that generate H_2O_2, which is subsequently reduced on the TiO_2 NPs surface. In contrast, the pernigraniline base form of PANI (present in the PANIox/TiO_2 film) has a detrimental effect on e^- transfer, and thus in the PEC performance for the water oxidation reaction. The PANI/TiO_2 film showed also an exceptional electrochemical durability under illumination for more than 190 min, moreover confirming the good adhesion of the composite material to the substrate. Such findings could also be useful to focus further research in order to still improve the here reported results, for instance by improving the PANI interpenetration in the TiO_2 porous films, and opens useful insights for future developments.

In Conclusion, a green and low-cost synthesis procedure was developed for the preparation of effective PANI/TiO_2 composite films, having a high surface nanocrystalline and mesoporous structure, which can find promising application not only in the PEC water splitting reaction, but also in other environmental photocatalytic applications in different redox systems.

Acknowledgements

The financial support from the European Commission on the 7th Framework Program NMP-2012 Project Eco^{2}CO$_2$ (no. 309701) and FCH- JU Call 2011-1 Project ARTIPHYCTION (no. 303435) is gratefully acknowledged.

Notes and references

1 J. A. Turner, *Science*, 2004, **305**, 972–974.
2 J. Gu, Y. Yan, J. W. Krizan, Q. D. Gibson, Z. M. Detweiler, R. J. Cava and A. B. Bocarsly, *J. Am. Chem. Soc.*, 2014, **136**, 830–833.
3 A. Fujishima and K. Honda, *Nature*, 1972, **238**, 37–38.
4 X. Hu, G. Li and J. C. Yu, *Langmuir*, 2009, **26**, 3031–3039.
5 D. Fattakhova-Rohlfing, A. Zaleska and T. Bein, *Chem. Rev.*, 2014, **114**, 9487–9558.
6 X. Chen and S. S. Mao, *Chem. Rev.*, 2007, **107**, 2891–2959.
7 C. Yu, B. Tian and D. Zhao, *Curr. Opin. Solid State Mater. Sci.*, 2003, **7**, 191–197.
8 M. L. K. Hoa, M. Lu and Y. Zhang, *Adv. Colloid Interface Sci.*, 2006, **121**, 9–23.
9 D. Hidalgo, R. Messina, A. Sacco, D. Manfredi, S. Vankova, E. Garrone, G. Saracco and S. Hernández, *Int. J. Hydrogen Energy*, 2014, **39**, 21512–21522.
10 C. Boissiere, D. Grosso, A. Chaumonnot, L. Nicole and C. Sanchez, *Adv. Mater.*, 2011, **23**, 599–623.
11 P. Innocenzi and L. Malfatti, *Chem. Soc. Rev.*, 2013, **42**, 4198–4216.
12 R. Zhang, A. A. Elzatahry, S. S. Al-Deyab and D. Zhao, *Nano Today*, 2012, **7**, 344–366.
13 M. C. Orilall and U. Wiesner, *Chem. Soc. Rev.*, 2011, **40**, 520–535.
14 W. Li and D. Zhao, *Adv. Mater.*, 2013, **25**, 142–149.
15 F. Zhu, D. Wu, Q. Li, H. Dong, J. Li, K. Jiang and D. Xu, *RSC Adv.*, 2012, **2**, 11629–11637.
16 J. B. Joo, Q. Zhang, M. Dahl, F. Zaera and Y. Yin, *J. Mater. Res.*, 2013, **28**, 362–368.
17 Q. Xiang, J. Yu and M. Jaroniec, *Nanoscale*, 2011, **3**, 3670–3678.
18 W. Zhou, H. Liu, R. I. Boughton, G. Du, J. Lin, J. Wang and D. Liu, *J. Mater. Chem.*, 2010, **20**, 5993–6008.
19 W. S. Tung and W. A. Daoud, *J. Mater. Chem.*, 2011, **21**, 7858–7869.
20 N. Liu, X. Chen, J. Zhang and J. W. Schwank, *Catal. Today*, 2014, **225**, 34–51.
21 P. Roy, S. Berger and P. Schmuki, *Angew. Chem., Int. Ed.*, 2011, **50**, 2904–2939.
22 A. Lamberti, A. Sacco, S. Bianco, D. Manfredi, F. Cappelluti, S. Hernandez, M. Quaglio and C. F. Pirri, *Phys. Chem. Chem. Phys.*, 2013, **15**, 2596–2602.
23 J. Yue, Z. H. Wang, K. R. Cromack, A. J. Epstein and A. G. MacDiarmid, *J. Am. Chem. Soc.*, 1991, **113**, 2665–2671.
24 D. P. Debecker, V. Hulea and P. H. Mutin, *Appl. Catal., A*, 2013, **451**, 192–206.
25 W. Zhou and H. Fu, *ChemCatChem*, 2013, **5**, 885–894.
26 H. Tong, S. Ouyang, Y. Bi, N. Umezawa, M. Oshikiri and J. Ye, *Adv. Mater.*, 2012, **24**, 229–251.
27 X. Wang and R. A. Caruso, *J. Mater. Chem.*, 2011, **21**, 20–28.
28 J. Z. Zhang, *MRS Bull.*, 2011, **36**, 48–55.
29 L. Jing, Z.-Y. Yang, Y.-F. Zhao, Y.-X. Zhang, X. Guo, Y.-M. Yan and K.-N. Sun, *J. Mater. Chem. A*, 2014, **2**, 1068–1075.
30 J. Wei, Q. Zhang, Y. Liu, R. Xiong, C. Pan and J. Shi, *J. Nanopart. Res.*, 2011, **13**, 3157–3165.
31 M. Qorbani, N. Naseri, O. Moradlou, R. Azimirad and A. Z. Moshfegh, *Appl. Catal., B*, 2015, **162**, 210–216.
32 S. Kuang, L. Yang, S. Luo and Q. Cai, *Appl. Surf. Sci.*, 2009, **255**, 7385–7388.
33 F. Deng, L. Min, X. Luo, S. Wu and S. Luo, *Nanoscale*, 2013, **5**, 8703–8710.
34 D. Pei and J. Luan, *Int. J. Photoenergy*, 2012, **2012**, 13.
35 W. J. Youngblood, S.-H. A. Lee, K. Maeda and T. E. Mallouk, *Acc. Chem. Res.*, 2009, **42**, 1966–1973.
36 G. Cai, J. Tu, D. Zhou, J. Zhang, Q. Xiong, X. Zhao, X. Wang and C. Gu, *J. Phys. Chem. C*, 2013, **117**, 15967–15975.
37 A. G. MacDiarmid and A. J. Epstein, *Faraday Discuss. Chem. Soc.*, 1989, **88**, 317–332.
38 J.-C. Chiang and A. G. MacDiarmid, *Synth. Met.*, 1986, **13**, 193–205.
39 A. MacDiarmid, J. Chiang, A. Richter and A. Epstein, *Synth. Met.*, 1987, **18**, 285–290.
40 A. G. MacDiarmid, *Angew. Chem., Int. Ed.*, 2001, **40**, 2581–2590.
41 A. G. MacDiarmid, J.-C. Chiang, A. F. Richter, N. L. D. Somasiri and A. J. Epstein, *Conducting Polymers*, ed. L. AlcaceÂr, Reidel, Dordrecht, 1987, p. 105.
42 S. Bocchini, A. Chiolerio, S. Porro, D. Accardo, N. Garino, K. Bejtka, D. Perrone and C. Pirri, *J. Mater. Chem. C*, 2013, **1**, 5101–5109.
43 A. Chiolerio, S. Bocchini and S. Porro, *Adv. Funct. Mater.*, 2014, **24**, 3472.
44 G. A. O. Jinzhang, L. I. Shengying, Y. Wu, Z. Guohu, B. O. Lili and S. Li, *Rare Met.*, 2007, **26**, 1–7.

45 M. Radoičić, Z. Šaponjić, I. A. Janković, G. Ćirić-Marjanović, S. P. Ahrenkiel and M. I. Čomor, *Appl. Catal., B*, 2013, **136–137**, 133–139.
46 J. Li, L. Zhu, Y. Wu, Y. Harima, A. Zhang and H. Tang, *Polymer*, 2006, **47**, 7361–7367.
47 X. Li, D. Wang, G. Cheng, Q. Luo, J. An and Y. Wang, *Appl. Catal., B*, 2008, **81**, 267–273.
48 H. Zhang, R. Zong, J. Zhao and Y. Zhu, *Environ. Sci. Technol.*, 2008, **42**, 3803–3807.
49 M. O. Ansari, M. M. Khan, S. A. Ansari, K. Raju, J. Lee and M. H. Cho, *ACS Appl. Mater. Interfaces*, 2014, **6**, 8124–8133.
50 G. Senadeera, T. Kitamura, Y. Wada and S. Yanagida, *J. Photochem. Photobiol., A*, 2004, **164**, 61–66.
51 K. He, M. Li and L. Guo, *Int. J. Hydrogen Energy*, 2012, **37**, 755–759.
52 T. Abdiryim, Z. Xiao-Gang and R. Jamal, *Mater. Chem. Phys.*, 2005, **90**, 367–372.
53 P. Madhu Kumar, S. Badrinarayanan and M. Sastry, *Thin Solid Films*, 2000, **358**, 122–130.
54 J. Tang, X. Jing, B. Wang and F. Wang, *Synth. Met.*, 1988, **24**, 231–238.
55 G. D'Aprano, M. Leclerc and G. Zotti, *Macromolecules*, 1992, **25**, 2145–2150.
56 J. J. Kelly, Z. Hens, D. Vanmaekelbergh and Z. Hensalso, in *Encyclopedia of electrochemistry*, Wiley-VCH Verlag GmbH & Co. KGaA, 2007, DOI: 10.1002/9783527610426.bard060201.
57 Z. Zhang and P. Wang, *Energy Environ. Sci.*, 2012, **5**, 6506–6512.
58 S. Hernandez, D. Hidalgo, A. Sacco, A. Chiodoni, A. Lamberti, V. Cauda, E. Tresso and G. Saracco, *Phys. Chem. Chem. Phys.*, 2015, **17**, 7775–7786.
59 M.-S. Liu, Y.-Z. Hao, X.-B. Qiao, M. Yang, M. Cai and Y. Li, *Electrochemistry*, 1998, **4**, 246.
60 G. Liao, S. Chen, X. Quan, Y. Zhang and H. Zhao, *Appl. Catal., B*, 2011, **102**, 126–131.
61 P. Akhter, M. Hussain, G. Saracco and N. Russo, *Fuel*, 2015, **149**, 55–65.
62 J. R. Harbour, J. Tromp and M. L. Hair, *Can. J. Chem.*, 1985, **63**, 204–208.
63 B. Jenny and P. Pichat, *Langmuir*, 1991, **7**, 947–954.
64 I. Ilisz, K. Föglein and A. Dombi, *J. Mol. Catal. A: Chem.*, 1998, **135**, 55–61.
65 A. Lamberti, A. Sacco, D. Hidalgo, S. Bianco, D. Manfredi, M. Quaglio, E. Tresso and C. F. Pirri, *Acta Phys. Pol., A*, 2013, **123**, 376.
66 S. Hernández, V. Cauda, A. Chiodoni, S. Dallorto, A. Sacco, D. Hidalgo, E. Celasco and C. F. Pirri, *ACS Appl. Mater. Interfaces*, 2014, **6**, 12153–12167.
67 S. Hernández, V. Cauda, D. Hidalgo, V. Farías Rivera, D. Manfredi, A. Chiodoni and F. C. Pirri, *J. Alloys Compd.*, 2014, **615**, S530–S537.
68 C. Belabed, A. Abdi, Z. Benabdelghani, G. Rekhila, A. Etxeberria and M. Trari, *Int. J. Hydrogen Energy*, 2013, **38**, 6593–6599.
69 W. Huang and A. MacDiarmid, *Polymer*, 1993, **34**, 1833–1845.
70 A. J. Bard and L. R. Faulkner, *Electrochemical Methods: Fundamentals and Applications*, Wiley, 2000.
71 K. Rajeshwar, in *Encyclopedia of electrochemistry*, Wiley-VCH Verlag GmbH & Co. KGaA, 2002.